metals

MDPI

Article

Mechanical Behavior and In Vitro Corrosion of Cubic Scaffolds of Pure Magnesium Processed by Severe Plastic Deformation

Claudio L. P. Silva [1,2], Marcelo A. Camara [3], Anton Hohenwarter [4] and Roberto B. Figueiredo [1,*]

[1] Department of Metallurgical and Materials Engineering, Universidade Federal de Minas Gerais, Av. Antônio Carlos 6627, Belo Horizonte 30270-901, Brazil; claudiolaudares@gmail.com
[2] Center of Technology in Nanomaterials and Graphene (CTNano–UFMG), Rua Professor José Vieira de Mendonça 520, Belo Horizonte 31310-260, Brazil
[3] Department of Mechanical Engineering, Universidade Federal de Minas Gerais, Av. Antônio Carlos 6627, Belo Horizonte 30270-901, Brazil; marcelocamara@demec.ufmg.br
[4] Department of Materials Science, Chair of Materials Physics, Montanuniversität Leoben, Jahnstraße 12, 8700 Leoben, Austria; anton.hohenwarter@unileoben.ac.at
* Correspondence: figueiredo@demet.ufmg.br

Abstract: Reports in the literature show that severe plastic deformation can improve mechanical strength, ductility, and corrosion resistance of pure magnesium, which suggests good performance for biodegradable applications. However, the reported results were based on testing of small samples on limited directions. The present study reports compression testing of larger samples, at different directions, in pure magnesium processed by hot rolling, equal channel angular pressing (ECAP), and high pressure torsion (HPT). The results show that severe plastic deformation through ECAP and HPT reduces anisotropy and increases strength and strain rate sensitivity. Also, scaffolds were fabricated from the material with different processing histories and immersed in Hank's solution for up to 14 days. The as-cast material displays higher corrosion rate and localized corrosion and it is reported that severe plastic deformation induces uniform corrosion and reduces the corrosion rate.

Keywords: magnesium; biodegradable material; scaffold; severe plastic deformation; mechanical properties

Citation: Silva, C.L.P.; Camara, M.A.; Hohenwarter, A.; Figueiredo, R.B. Mechanical Behavior and In Vitro Corrosion of Cubic Scaffolds of Pure Magnesium Processed by Severe Plastic Deformation. *Metals* **2021**, *11*, 1791. https://doi.org/10.3390/met11111791

Academic Editor: Asit Kumar Gain

Received: 16 September 2021
Accepted: 4 November 2021
Published: 8 November 2021

1. Introduction

Magnesium and its alloys are considered leading metallic materials for bio-degradable applications due to a combination of biocompatibility, corrosion rate, and mechanical properties. Recent papers reviewed the advances in the general use of magnesium [1], the progress in in vivo studies [2] and the use of magnesium for bone repair and regeneration [3]. Scaffolds, which are porous implant structures, display great potential for tissue regeneration [4] and orthopedic applications [5]. The interconnected pores allow tissue ingrowth and facilitate the transport of oxygen, nutrients, and byproducts of cell metabolism [6]. Many parameters affect the performance of these devices including the porosity fraction, geometry, and distribution of pores. Some of the requirements and advances in scaffold design for orthopedic implants have been reviewed [5]. Typical scaffolds types are described in the literature [5], including functionally graded porous scaffolds [7].

Yet, the fabrication of magnesium scaffolds with controlled degree of porosity remains a challenge due to the requirement of connection between the pores and minimum diameter without compromising the overall structural integrity. Some of the techniques that have been used to produce magnesium scaffolds include additive manufacturing [8] and space holder techniques such as negative salt pattern molding [9–12] or entangled titanium wires [13]. These techniques prevent the use of thermo-mechanical processing to improve the properties of the material. Other fabrication techniques that can be used to produce scaffolds from wrought magnesium include electrical discharge drilling [14], laser drilling [15], and conventional drilling [16,17].

Research in recent years has focused on tailoring composition and processing operations that will optimize the performance of magnesium, which include improvement in biological response to the material, controlling corrosion type and corrosion rate, and improving strength and ductility. It is known that pure magnesium exhibits good biocompatibility and in vivo experiments showed good biological response to magnesium implants [18,19]. The corrosion behavior of magnesium depends on purity levels [20] and, therefore, the experimental results vary significantly. One of the main constraints for the use of pure magnesium as a biodegradable implant is its low mechanical strength. In addition, ductility of magnesium and its alloys might be an issue for applications in which plastic deformation can be expected.

Thermo-mechanical processing is a common way to change the structure and improve mechanical properties of metallic materials in general and it is also effective for magnesium and its alloys. Also, thermo-mechanical processing seems to improve corrosion resistance and an example of this trend is the decrease in corrosion rate observed in dilute magnesium binary alloys after processing by hot rolling [21]. Therefore, it is of great interest to evaluate the effect of thermo-mechanical processing in the performance of magnesium for biological applications.

Severe plastic deformation (SPD) has attracted significant attention in recent decades, as processing operations are able to refine the grain structure of metallic materials more effectively than conventional thermo-mechanical processes such as rolling and extrusion. The finer grains produced by SPD are associated with improved mechanical strength [22,23] and recent papers have shown that exceptional ductility is observed in ultrafine grained pure magnesium [24,25]. On top of the improvements in mechanical properties, it has been proved that rolling, equal-channel angular pressing (ECAP) [26], and high pressure torsion (HPT) [27] processing do not compromise biocompatibility and may improve corrosion resistance [28–30].

Although the results reported in the literature show that HPT processing displays extraordinary potential to improve the performance of magnesium for biodegradable applications, some sample size issues remain as a concern as it can impact the materials' response in some tests. For example, most of the data on mechanical strength of samples of magnesium processed by HPT were collected from microhardness tests [31,32] or tensile tests in miniature samples [25,30] in which the loading direction is usually parallel to the disc rotation direction. This can impact the results since it is known that the mechanical behavior of magnesium is anisotropic and strength and ductility depends on sample direction [33,34]. Also, it is known that electrochemical tests are not an appropriate method to estimate corrosion rate in magnesium and hydrogen evolution tests can be affected by sample size. Therefore it is possible that the corrosion rates reported in the literature underestimate the real values for samples processed by HPT, which usually display less than 1 mm in thickness. Thus, the present work aims to clarify these points by carrying out compression tests at different directions in larger samples of pure magnesium processed by rolling, ECAP, and HPT and by evaluation of the corrosion rate in a real scaffolds with high surface area. These processing routes were selected because a previous study showed they can significantly alter the microstructure, mechanical properties, and corrosion behavior of pure magnesium [29].

2. Materials and Methods

The material used in the present experiments was commercial purity magnesium (>99.7%) provided by Rima (Bocaiúva-MG/Brazil). The material was received in the as-cast condition. A sheet with ~8 mm thickness was cut and rolled, at ~100 mm/s, to ~4 mm thickness in multiple passes. The sheet was heated in a furnace at 673 K for 10 min before each rolling step. After reaching the target thickness, the sheet was air cooled to room temperature.

A sheet was rolled to 5 mm thickness, cut into $5 \times 10 \times 60$ mm^3 slabs, cleaned using acetone, and stacked to produce a 10×10 mm^2 cross section. The stacked sheets were processed by 4 passes of ECAP using a die with 135° between channels. The ECAP die was heated to 473 K and the material was inserted 10 min before ECAP processing in order to homogenize the temperature with the die. ECAP processing was carried out for 4 passes with a 180° rotation between passes. No bonding is observed between the slabs during ECAP processing and the $5 \times 10 \times 60$ mm^3 samples were used in the investigation.

Additionally, discs with 30 mm diameter and 7.5 mm thickness were machined from the as cast material and processed by HPT to 5 turns using a quasi-constrained machine operating at a nominal pressure of 2 GPa at room temperature.

Compression tests were carried out from samples extracted at different directions from the rolled sheet, ECAP processed billets and HPT processed discs. A total of 8 different conditions were evaluated. Figure 1 illustrates the direction and nomenclature for the compression specimens. The specimens had different dimensions, but a height to thickness ratio of 1.5 was maintained. The dimensions of the smallest specimen were $2.6 \times 2.6 \times 4.0$ mm^3 and the dimensions of the largest were $5.0 \times 5.0 \times 7.5$ mm^3. The tests were carried out with different initial cross head displacement, i.e., strain rates. A total of 21 tests were carried out to evaluate the effect of processing history, direction and strain rate. The load and displacement data were converted to stress and strain considering homogeneous deformation. The elastic portion of the stress vs. strain curves were associated to the elastic modulus of magnesium in order to take the elastic distortion of the machine into account.

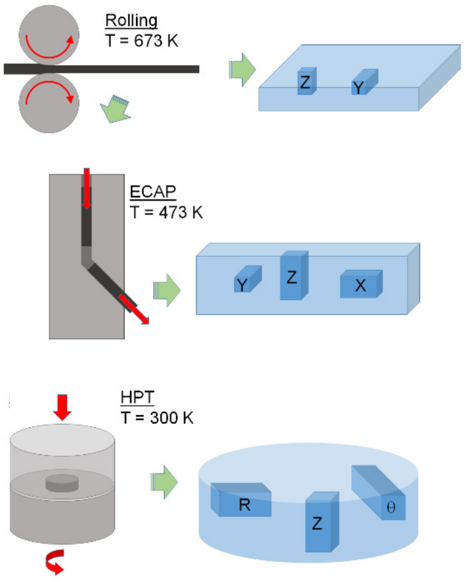

Figure 1. Illustration of the direction of compression specimens machined from the different samples.

Six scaffolds were produced by machining of the as-cast, rolled, ECAP, and HPT processed materials. Machining allows the control of dimensions of holes and degree of porosity and can produce interconnected holes. The cubic specimens had ~4 mm edges. Holes were drilled in the cubic specimens using 4 steps of 1 mm depth drilling each. The drilling was carried out at 6000 rpm and 100 mm/min. Two tools were used to produce 1 or 0.5 mm diameter holes. Care was taken during drilling to produce continuous and intersecting holes.

Thus, 4 cubic scaffolds with 4 holes with 0.5 mm diameter in each face were produced from the as-cast, rolled, ECAP, and HPT processed materials. Additionally, 2 cubic scaffolds with 1 hole with 1.0 mm diameter in each face were produced from the as-cast and the material processed by ECAP. The scaffolds were immersed in a solution of 10% nitric acid with 90% ethanol to remove residues of the machining processes and to attain a polished surface. Figure 2 shows the appearance of a scaffold in which 4 holes with 0.5 mm diameter were drilled in each surface.

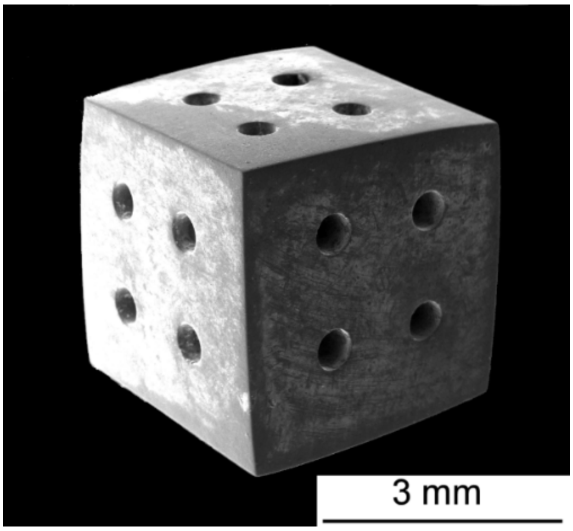

Figure 2. Example of a cubic scaffold, with 0.5 mm holes, used in the present investigation.

Each scaffold was immersed in approximately 200 mL of Hank's solution for 14 days at room temperature. A funnel was used to collect H_2 and the volume of gas was used to estimate the corrosion rate. A detailed description of this experimental technique is available elsewhere [35]. The volume of hydrogen, V_{H_2}, was tracked and related to the mass loss of magnesium, m, using Equation (1).

$$m = \frac{PV_{H_2}}{RT} \times M_{\mathrm{Mg}} \quad (1)$$

where P is the gas pressure, R is the universal gas constant, T is the absolute temperature, and M_{Mg} is the molar mass of Mg. The corrosion penetration rate, CR, was calculated using Equation (2).

$$PR = \frac{m_{\mathrm{Mg}}}{St} \quad (2)$$

where S is the surface area and t is the time of exposure. Corroded samples were observed in a scanning electron microscope after 14 days.

3. Results

3.1. Compression Tests

Figure 3 shows the stress vs. strain curves for tests with initial strain rate of 10^{-4}, 10^{-3}, and 10^{-2} s^{-1} in the material with different processing histories. A curve obtained for this material in the as-cast condition [36] is also shown, together with the curves of the material processed by rolling, for comparison. A significant anisotropy, different mechanical response at different testing direction, is observed in the material processed by hot rolling. Processing by rolling is known to develop a characteristic texture in which a large fraction of the basal planes of the h.c.p. structure becomes parallel to the sheet plane [37,38]. Therefore, it is expected that the compression axis will be nearly parallel to the c-axis for most of the grains and twinning can be suppressed for tests along the Z direction. As a consequence, the material displays a high strength in this direction. On the other hand, twinning is expected to play a major role during compression along the Y direction. The results show low yield stress and sigmoidal curves in this condition, which is considered as a twinning signature [39–42]. The shape of the curves agree with what was reported in a hot rolled AZ31 magnesium alloy subjected to compression at similar directions [38].

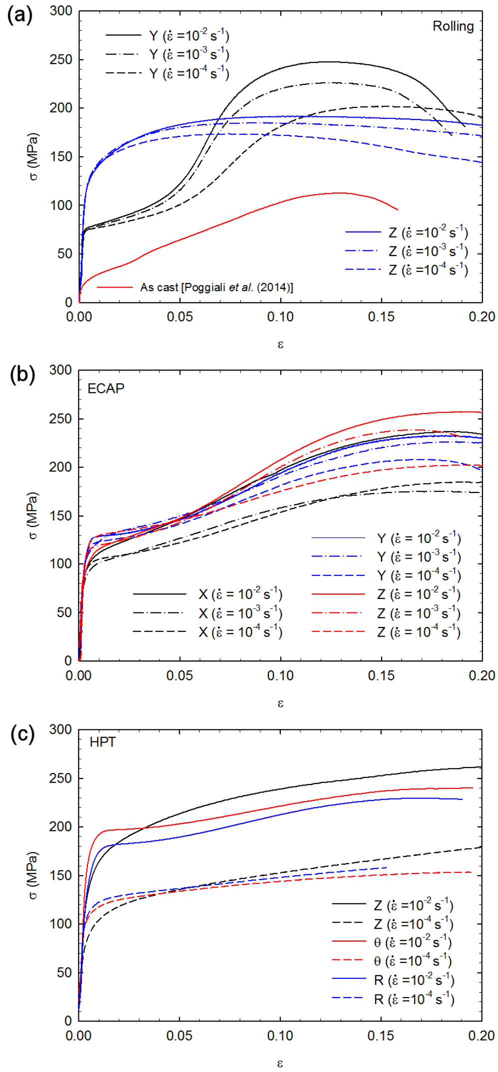

Figure 3. Compression stress vs. strain curves obtained at different loading directions and strain rates for the pure magnesium processed by (**a**) rolling, (**b**) ECAP, and (**c**) HPT.

The anisotropy seems to decrease in the material processed by ECAP and testing along the three orthogonal directions reveal yield stress within a narrow range of 100~130 MPa. Careful inspection shows that all curves display an increase in slope at a strain of ~0.05, which suggests twinning is active in this material tested in these conditions.

Compression tests were carried out at only two different strain rates in the material processed by HPT due to a reduced number of samples in this condition. The curves for tests at 10^{-2} s^{-1} show a continuous decrease in slope for testing along direction Z and sigmoidal shape curves for testing along R and θ directions. This suggests twinning signature is only observed along R and θ directions and dislocation slip controls deformation along Z direction. HPT processing is known to produce a similar texture as in hot rolling in which the basal planes of the majority of the grains tend to align parallel to the disc surface [23,43]. Therefore, the shape of the curves agree with the observed in the rolled material. However, it is apparent that the yield anisotropy is lower in this material compared to the hot rolled material. It is also interesting to note that all curves display a significant decrease in the level of flow stress and a continuous decrease in slope when testing at 10^{-4} s^{-1}. This shows that this material display a significant strain-rate sensitivity and suggests that decreasing the strain rate prevents twinning in this material.

Additional tests were carried out using a low strain rate of 10^{-6} s^{-1} in five samples and Figure 4 shows the curves obtained. The curves from the material processed by ECAP show no indication of twinning activity. It seems that the material displays a near perfect plastic behavior when tested along directions Y and Z in which deformation takes place under a constant flow stress level. The curve for the sample tested along the X direction shows a slight strain-hardening behavior in which the strain hardening rate decreases with increasing strain. A similar behavior was observed in the material processed by HPT and tested along the Z direction, although the level of flow stress is significantly lower. It is interesting to note that the flow stress is larger for the sample processed by hot rolling and smaller for the HPT processed material. This is attributed to the structure refinement produced by SPD. It has been shown that pure magnesium displays inverse Hall-Petch behavior at very fine grain sizes when tested at low strain rates [44,45].

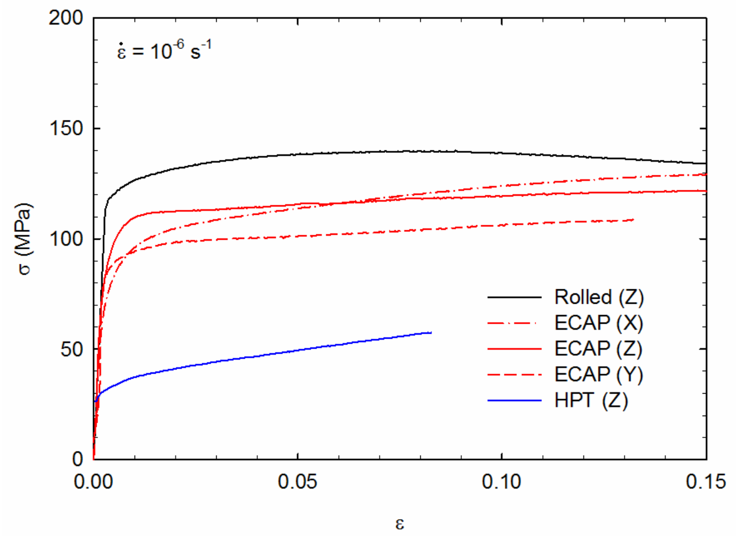

Figure 4. Stress vs. strain curves obtained for pure magnesium processed by rolling, ECAP, and HPT tested at $10^{-6}\ s^{-1}$.

3.2. Immersion Tests

Cubic scaffolds with 4 mm edge were immersed in Hank's solution for 14 days and the volume of hydrogen produced by corrosion is shown in Figure 5, after being normalized by the exposed area of each sample. The calculated corrosion penetration rate is also shown. The data for a small disc sample of the as-cast material from the literature [28] is also shown for comparison. The results show that the scaffold produced from the as-cast material corrodes faster than its counterpart processed by rolling and severe plastic deformation. The total volume of hydrogen produced during corrosion is ~10× larger in the former. There is only a minor difference between the amount of hydrogen produced during corrosion of scaffolds produced from the material processed by rolling, ECAP, or HPT. The corrosion penetration rate in these materials vary slightly, but are limited to less than ~0.4 mm/year.

It is important to note there is a significant difference in volume of hydrogen, normalized by the sample surface area, in samples of the as-cast material with different shapes and exposed surface areas. It is apparent that the amount of hydrogen decreases with decreasing sample surface area as it decreases with decreasing the number of holes on the scaffold and a 10 mm diameter thin disc [28], which display the lowest surface area, also display the lowest volume of hydrogen. This is attributed to a sample size effect in this test. Some of the hydrogen produced during corrosion is dissolved in the Hank's solution and released to the environment outside of the funnel. This leads to underestimation of the corrosion rate. This affects significantly the results from tests of small samples with reduced surface area.

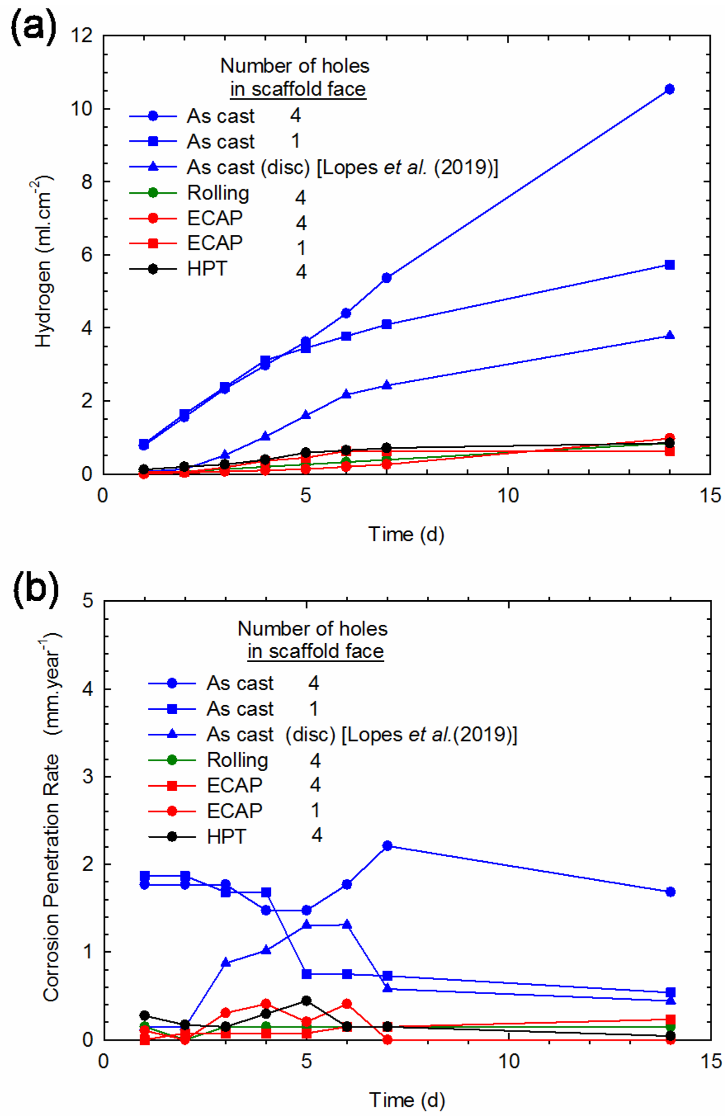

Figure 5. (**a**) Volume of hydrogen produced during immersion and (**b**) corrosion penetration rate of different samples plotted as a function of the immersion time.

Figure 6 shows the appearance of the scaffolds after being immersed in Hank's solution for 14 days. The as-cast material displays the highest damage with largest volume of material being corroded. Also, the corrosion in this case seems localized as a corner of the sample was totally corroded during immersion and the remaining of the scaffold underwent much lower corrosion. The scaffolds produced from the processed materials preserve the original shape, which suggests these materials undergo uniform corrosion. However, it is important to note that the corrosion products filled the holes in the scaffold produced from the rolled material and it seems the holes are still preserved in the materials processed by severe plastic deformation (ECAP and HPT). EDS analysis of the composition of the corrosion product layer that covered the surface of the scaffolds reveal significant amounts of C, O, Na, Mg, P, and Ca. This shows that elements from the solution are deposited on the surfaces of the magnesium scaffolds. Similar composition of corrosion product layer has been reported in pure magnesium immersed in Hank's solution with glucose [46]. However, mainly Mg and O are present in the area in which localized corrosion took place in the scaffold produced from the as-cast material, suggesting that the elements absorbed from the solution might aid on developing a protective surface layer and preventing localized corrosion.

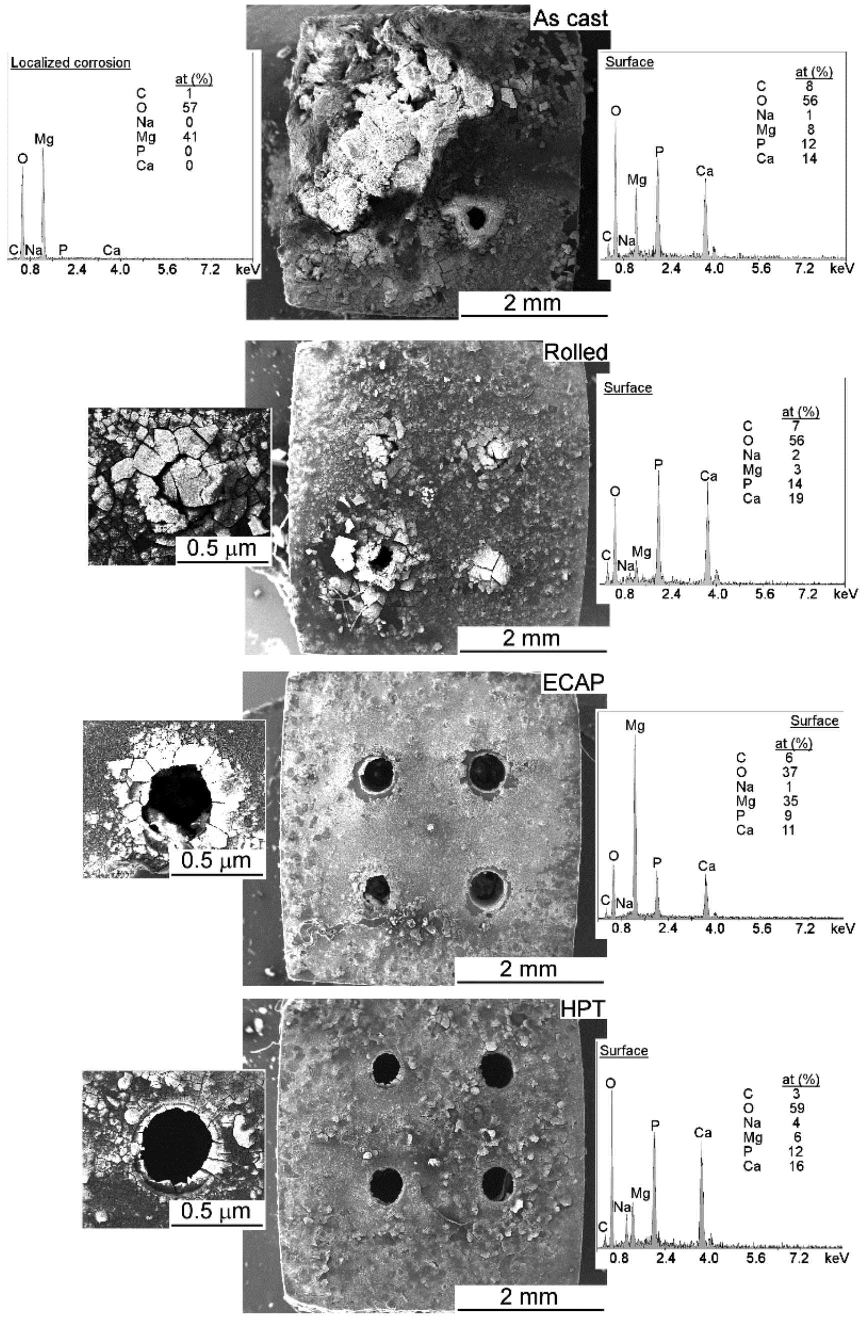

Figure 6. Appearance of scaffolds fabricated from pure magnesium in the as-cast condition and after processing by rolling, ECAP, and HPT. EDS analysis of composition of the surface of the corroded scaffolds are also presented.

4. Discussion

It is known that the compression behavior of coarse grained polycrystalline magnesium and its alloys depends on previous processing and texture and is anisotropic [33,36]. Also, significant difference in stress vs. strain curves are observed in similar materials when tested in tension or compression [41,42,47]. Although some differences are noted when comparing the present curves with a previous report in which tensile tests were used to determine the mechanical behavior of pure magnesium in the as cast condition and after processing by hot rolling, ECAP, and HPT [29], it is clear that yield stresses of ~100 MPa can be obtained in pure magnesium after processing by severe plastic deformation. This is significantly larger than the observed in the as-cast material. Also, the present results show that such strength does not depend on loading direction, as it is apparent that anisotropy decreases in the material processed by SPD.

On the other hand, the gain in strength is observed in samples tested in the strain rate range 10^{-4}~10^{-2} s^{-1} and a significant drop in strength is observed in the material processed by HPT when tested at a very low strain rate of 10^{-6} s^{-1}. This shows that processing by HPT can reduce the resistance for applications in which the material is subjected to long periods of loading. Such decrease in strength at this low strain rate is not observed in the material processed by ECAP though. This shows that optimization of the SPD processing is important to attain the best performance in magnesium. The present results confirm that the hydrogen evolution test depends strongly on sample size. The results for the as-cast material showed more than a two-fold increase in the volume of hydrogen per area in the sample with larger volume and larger exposed area. Still, the material processed by rolling, ECAP, and HPT display a very low corrosion rate in the tests with large samples, which confirm that thermo-mechanical processing improves corrosion resistance. The main observation of the present results though is that the processed samples did not display signs of localized corrosion. This is clearly observed in the scaffolds fabricated from the material processed by SPD (ECAP and HPT), which maintain the shape and open holes after 14 days of immersion in Hank's solution. This observation agrees with the suggestion of occurrence of a pseudo-uniform corrosion in materials processed by SPD [48] and confirms previous observations of uniform corrosion in small samples of pure magnesium processed by HPT [28]. It is important to note that a decrease in corrosion resistance was reported in pure magnesium after processing by HPT [30]. This opposite trend in the present study might be attributed to composition effects since it is known that minor differences in composition and purity can affect significantly the corrosion resistance of magnesium [20].

5. Conclusions

Commercial purity magnesium was processed by hot rolling, ECAP, and HPT from the as-cast condition. Compression tests at different directions and strain rates were carried out and scaffolds were fabricated from the different materials and subjected to immersion in Hank's solution.

The material processed by hot rolling displays significant anisotropy in mechanical behavior and low strain rate sensitivity. The material processed by rolling followed by ECAP displays lower anisotropy and a higher strain rate sensitivity. The material processed by HPT shows low anisotropy and the highest strain rate sensitivity.

An improvement in strength is obtained by processing magnesium using SPD techniques, but the material processed by HPT displays a reduced resistance at a very low strain rate of 10^{-6} s^{-1}.

Hydrogen evolution test shows a large dependence on the sample size. The samples processed by hot rolling, ECAP, and HPT display a significantly higher corrosion resistance compared to the as-cast material.

The scaffold fabricated from the as-cast material underwent localized corrosion and lost its shape after 14 days of immersion in Hank's solution. The scaffolds produced from the material processed by SPD (ECAP and HPT) show high corrosion resistance, maintained its shape, and the scaffold holes were still open after 14 days of immersion.

Author Contributions: Conceptualization, C.L.P.S.; Investigation, C.L.P.S.; Writing—review and editing, C.L.P.S., M.A.C., A.H. and R.B.F. All authors have read and agreed to the published version of the manuscript.

Funding: R.B.F. acknowledges financial support from CNPq (grant #302445/2018-8) and FAPEMIG (grant TEC-PPM-00324-17).

Data Availability Statement: The data that support the findings of this study are available from the corresponding author, upon reasonable request.

Conflicts of Interest: The authors declare no conflict of interest.

References

1. Yang, Y.; Xiong, X.; Chen, J.; Peng, X.; Chen, D.; Pan, F. Research advances in magnesium and magnesium alloys worldwide in 2020. *J. Magnes. Alloys* **2021**, *9*, 705–747. [CrossRef]
2. Sekar, P.; Narendranath, S.; Desai, V. Recent progress in in vivo studies and clinical applications of magnesium based biodegradable implants—A review. *J. Magnes. Alloys* **2021**, *9*, 1147–1163. [CrossRef]
3. Zhou, H.; Liang, B.; Jiang, H.; Deng, Z.; Yu, K. Magnesium-based biomaterials as emerging agents for bone repair and regeneration: From mechanism to application. *J. Magnes. Alloys* **2021**, *9*, 779–804. [CrossRef]
4. Hollister, S.J. Porous scaffold design for tissue engineering. *Nat. Mater.* **2005**, *4*, 518–524. [CrossRef]
5. Wang, X.; Xu, S.; Zhou, S.; Xu, W.; Leary, M.; Choong, P.; Qian, M.; Brandt, M.; Xie, Y.M. Topological design and additive manufacturing of porous metals for bone scaffolds and orthopaedic implants: A review. *Biomaterials* **2016**, *83*, 127–141. [CrossRef]
6. Kamrani, S.; Fleck, C. Biodegradable magnesium alloys as temporary orthopaedic implants: A review. *BioMetals* **2019**, *32*, 185–193. [CrossRef] [PubMed]
7. Han, C.; Li, Y.; Wang, Q.; Wen, S.; Wei, Q.; Yan, C.; Hao, L.; Liu, J.; Shi, Y. Continuous functionally graded porous titanium scaffolds manufactured by selective laser melting for bone implants. *J. Mech. Behav. Biomed. Mater.* **2018**, *80*, 119–127. [CrossRef] [PubMed]
8. Sezer, N.; Evis, Z.; Koç, M. Additive manufacturing of biodegradable magnesium implants and scaffolds: Review of the recent advances and research trends. *J. Magnes. Alloys* **2021**, *9*, 392–415. [CrossRef]
9. Witte, F.; Ulrich, H.; Palm, C.; Willbold, E. Biodegradable magnesium scaffolds: Part II: Peri-implant bone remodeling. *J. Biomed. Mater. Res. Part A* **2007**, *81A*, 757–765. [CrossRef]
10. Witte, F.; Ulrich, H.; Rudert, M.; Willbold, E. Biodegradable magnesium scaffolds: Part 1: Appropriate inflammatory response. *J. Biomed. Mater. Res. Part A* **2007**, *81A*, 748–756. [CrossRef]
11. Kleger, N.; Cihova, M.; Masania, K.; Studart, A.R.; Löffler, J.F. 3D printing of salt as a template for magnesium with structured porosity. *Adv. Mater.* **2019**, *31*, 1903783. [CrossRef] [PubMed]
12. Dong, Q.; Li, Y.; Jiang, H.; Zhou, X.; Liu, H.; Lu, M.; Chu, C.; Xue, F.; Bai, J. 3D-cubic interconnected porous Mg-based scaffolds for bone repair. *J. Magnes. Alloys* **2021**, *9*, 1329–1338. [CrossRef]
13. Cheng, M.Q.; Wahafu, T.; Jiang, G.F.; Liu, W.; Qiao, Y.Q.; Peng, X.C.; Cheng, T.; Zhang, X.L.; He, G.; Liu, X.Y. A novel open-porous magnesium scaffold with controllable microstructures and properties for bone regeneration. *Sci. Rep.* **2016**, *6*, 24134. [CrossRef] [PubMed]
14. Ahuja, N.; Kumar, K.; Batra, U.; Garg, S.K. Fabrication of Biodegradable Mg Alloy Bone Scaffold Through Electrical Discharge µ-Drilling Route. In *Advances in Manufacturing II*; Springer: Cham, Switzerland, 2019; pp. 145–155.
15. Tan, L.; Gong, M.; Zheng, F.; Zhang, B.; Yang, K. Study on compression behavior of porous magnesium used as bone tissue engineering scaffolds. *Biomed. Mater.* **2009**, *4*, 015016. [CrossRef]
16. Liu, Y.J.; Yang, Z.Y.; Tan, L.L.; Li, H.; Zhang, Y.Z. An animal experimental study of porous magnesium scaffold degradation and osteogenesis. *Braz. J. Med. Biol. Res.* **2014**, *47*, 715–720. [CrossRef]
17. Basri, H.; Prakoso, A.T.; Sulong, M.A.; Md Saad, A.P.; Ramlee, M.H.; Agustin Wahjuningrum, D.; Sipaun, S.; Öchsner, A.; Syahrom, A. Mechanical degradation model of porous magnesium scaffolds under dynamic immersion. *Proc. Inst. Mech. Eng. Part L J. Mater. Des. Appl.* **2019**, *234*, 175–185. [CrossRef]
18. Chaya, A.; Yoshizawa, S.; Verdelis, K.; Myers, N.; Costello, B.J.; Chou, D.-T.; Pal, S.; Maiti, S.; Kumta, P.N.; Sfeir, C. In vivo study of magnesium plate and screw degradation and bone fracture healing. *Acta Biomater.* **2015**, *18*, 262–269. [CrossRef]
19. Zainal Abidin, N.I.; Rolfe, B.; Owen, H.; Malisano, J.; Martin, D.; Hofstetter, J.; Uggowitzer, P.J.; Atrens, A. The in vivo and in vitro corrosion of high-purity magnesium and magnesium alloys WZ21 and AZ91. *Corros. Sci.* **2013**, *75*, 354–366. [CrossRef]
20. Cao, F.; Song, G.-L.; Atrens, A. Corrosion and passivation of magnesium alloys. *Corros. Sci.* **2016**, *111*, 835–845. [CrossRef]
21. Cao, F.; Shi, Z.; Song, G.-L.; Liu, M.; Dargusch, M.S.; Atrens, A. Influence of hot rolling on the corrosion behavior of several Mg–X alloys. *Corros. Sci.* **2015**, *90*, 176–191. [CrossRef]
22. Biswas, S.; Singh Dhinwal, S.; Suwas, S. Room-temperature equal channel angular extrusion of pure magnesium. *Acta Mater.* **2010**, *58*, 3247–3261. [CrossRef]
23. Figueiredo, R.B.; Langdon, T.G. Processing magnesium and its alloys by high-pressure torsion: An overview. *Adv. Eng. Mater.* **2019**, *21*, 1801039. [CrossRef]
24. Zeng, Z.; Nie, J.F.; Xu, S.W.; Davies, C.H.; Birbilis, N. Super-formable pure magnesium at room temperature. *Nat. Commun.* **2017**, *8*, 972. [CrossRef] [PubMed]
25. Figueiredo, R.B.; Sabbaghianrad, S.; Giwa, A.; Greer, J.R.; Langdon, T.G. Evidence for exceptional low temperature ductility in polycrystalline magnesium processed by severe plastic deformation. *Acta Mater.* **2017**, *122*, 322–331. [CrossRef]
26. Valiev, R.Z.; Langdon, T.G. Principles of equal-channel angular pressing as a processing tool for grain refinement. *Prog. Mater. Sci.* **2006**, *51*, 881–981. [CrossRef]
27. Zhilyaev, A.P.; Langdon, T.G. Using high-pressure torsion for metal processing: Fundamentals and applications. *Prog. Mater. Sci.* **2008**, *53*, 893–979. [CrossRef]
28. Lopes, D.R.; Silva, C.L.P.; Soares, R.B.; Pereira, P.H.R.; Oliveira, A.C.; Figueiredo, R.B.; Langdon, T.G.; Lins, V.F.C. Cytotoxicity and corrosion behavior of magnesium and magnesium alloys in Hank's solution after processing by high-pressure torsion. *Adv. Eng. Mater.* **2019**, *21*, 1900391. [CrossRef]

29. Silva, C.L.P.; Oliveira, A.C.; Costa, C.G.F.; Figueiredo, R.B.; de Fátima Leite, M.; Pereira, M.M.; Lins, V.F.C.; Langdon, T.G. Effect of severe plastic deformation on the biocompatibility and corrosion rate of pure magnesium. *J. Mater. Sci.* **2017**, *52*, 5992–6003. [CrossRef]
30. Li, W.; Liu, X.; Zheng, Y.; Wang, W.; Qiao, W.; Yeung, K.W.K.; Cheung, K.M.C.; Guan, S.; Kulyasova, O.B.; Valiev, R.Z. In vitro and in vivo studies on ultrafine-grained biodegradable pure Mg, Mg–Ca alloy and Mg–Sr alloy processed by high-pressure torsion. *Biomater. Sci.* **2020**, *8*, 5071–5087. [CrossRef]
31. Edalati, K.; Yamamoto, A.; Horita, Z.; Ishihara, T. High-pressure torsion of pure magnesium: Evolution of mechanical properties, microstructures and hydrogen storage capacity with equivalent strain. *Scr. Mater.* **2011**, *64*, 880–883. [CrossRef]
32. Silva, C.L.P.; Tristão, I.C.; Sabbaghianrad, S.; Torbati-Sarraf, S.A.; Figueiredo, R.B.; Langdon, T.G. Microstructure and hardness evolution in magnesium processed by HPT. *Mater. Res.* **2017**, *20*, 2–7. [CrossRef]
33. Agnew, S.R.; Horton, J.A.; Lillo, T.M.; Brown, D.W. Enhanced ductility in strongly textured magnesium produced by equal channel angular processing. *Scr. Mater.* **2004**, *50*, 377–381. [CrossRef]
34. Figueiredo, R.B.; Száraz, Z.; Trojanová, Z.; Lukáč, P.; Langdon, T.G. Significance of twinning in the anisotropic behavior of a magnesium alloy processed by equal-channel angular pressing. *Scr. Mater.* **2010**, *63*, 504–507. [CrossRef]
35. Song, G.; Atrens, A.; StJohn, D. An Hydrogen Evolution Method for the Estimation of the Corrosion Rate of Magnesium Alloys. In *Essential Readings in Magnesium Technology*; Springer: Cham, Switzerland, 2016; pp. 565–572.
36. Poggiali, F.S.J.; Silva, C.L.P.; Pereira, P.H.R.; Figueiredo, R.B.; Cetlin, P.R. Determination of mechanical anisotropy of magnesium processed by ECAP. *J. Mater. Res. Technol.* **2014**, *3*, 331–337. [CrossRef]
37. Cepeda-Jiménez, C.M.; Molina-Aldareguia, J.M.; Pérez-Prado, M.T. Effect of grain size on slip activity in pure magnesium polycrystals. *Acta Mater.* **2015**, *84*, 443–456. [CrossRef]
38. Guo, X.Q.; Chapuis, A.; Wu, P.D.; Agnew, S.R. On twinning and anisotropy in rolled Mg alloy AZ31 under uniaxial compression. *Int. J. Solids Struct.* **2015**, *64–65*, 42–50. [CrossRef]
39. Barnett, M.R.; Keshavarz, Z.; Beer, A.G.; Atwell, D. Influence of grain size on the compressive deformation of wrought Mg–3Al–1Zn. *Acta Mater.* **2004**, *52*, 5093–5103. [CrossRef]
40. Dixit, N.; Xie, K.Y.; Hemker, K.J.; Ramesh, K.T. Microstructural evolution of pure magnesium under high strain rate loading. *Acta Mater.* **2015**, *87*, 56–67. [CrossRef]
41. Knezevic, M.; Levinson, A.; Harris, R.; Mishra, R.K.; Doherty, R.D.; Kalidindi, S.R. Deformation twinning in AZ31: Influence on strain hardening and texture evolution. *Acta Mater.* **2010**, *58*, 6230–6242. [CrossRef]
42. Ulacia, I.; Dudamell, N.V.; Gálvez, F.; Yi, S.; Pérez-Prado, M.T.; Hurtado, I. Mechanical behavior and microstructural evolution of a Mg AZ31 sheet at dynamic strain rates. *Acta Mater.* **2010**, *58*, 2988–2998. [CrossRef]
43. Bonarski, B.J.; Schafler, E.; Mingler, B.; Skrotzki, W.; Mikulowski, B.; Zehetbauer, M.J. Texture evolution of Mg during high-pressure torsion. *J. Mater. Sci.* **2008**, *43*, 7513–7518. [CrossRef]
44. Somekawa, H.; Mukai, T. Hall–Petch breakdown in fine-grained pure magnesium at low strain rates. *Metall. Mater. Trans. A* **2015**, *46*, 894–902. [CrossRef]
45. Zheng, R.; Du, J.-P.; Gao, S.; Somekawa, H.; Ogata, S.; Tsuji, N. Transition of dominant deformation mode in bulk polycrystalline pure Mg by ultra-grain refinement down to sub-micrometer. *Acta Mater.* **2020**, *198*, 35–46. [CrossRef]
46. Zeng, R.-C.; Li, X.-T.; Li, S.-Q.; Zhang, F.; Han, E.-H. In vitro degradation of pure Mg in response to glucose. *Sci. Rep.* **2015**, *5*, 13026. [CrossRef]
47. Atwell, D.L.; Barnett, M.R.; Hutchinson, W.B. The effect of initial grain size and temperature on the tensile properties of magnesium alloy AZ31 sheet. *Mater. Sci. Eng. A* **2012**, *549*, 1–6. [CrossRef]
48. Miyamoto, H.; Yuasa, M.; Rifai, M.; Fujiwara, H. Corrosion behavior of severely deformed pure and single-phase materials. *Mater. Trans.* **2019**, *60*, 1243–1255. [CrossRef]